

Article

Effects of Aging, Cognitive Dysfunction, Brain Atrophy on Hemoglobin Concentrations and Optical Pathlength at Rest in the Prefrontal Cortex: A Time-Resolved Spectroscopy Study

Kaoru Sakatani ^{1,2,*}, Lizhen Hu ¹, Katsunori Oyama ³ and Yukio Yamada ⁴ 

¹ Laboratory of Universal Sport Health Sciences, Department of Human and Engineered Environmental Studies, Graduate School of Frontier Sciences, The University of Tokyo, Chiba 277-8561, Japan; lizhen_hu@hotmail.com

² Institute for Healthcare Robotics, Future Robotics Organization, Waseda University, Tokyo 169-8050, Japan

³ Department of Computer Science, College of Engineering, Nihon University, Fukushima 963-8642, Japan; oyama@cs.ce.nihon-u.ac.jp

⁴ Center for Neuroscience and Biomedical Engineering, The University of Electro-Communications, Tokyo 182-8585, Japan; yukioyamada@uec.ac.jp

* Correspondence: k.sakatani@edu.k.u-tokyo.ac.jp; Tel.: +81-4-7136-4613

Received: 9 April 2019; Accepted: 20 May 2019; Published: 29 May 2019



Featured Application: Time-resolved spectroscopy may be a useful tool for screening test of cognitive dysfunction in the elderly, particularly who cannot respond to cognitive tasks.

Abstract: Background: In order to evaluate usefulness of a time-resolved spectroscopy (TRS) in screening test of cognitive dysfunction, we studied the effects of aging, cognitive dysfunction, brain atrophy on hemoglobin (Hb) concentrations and optical pathlengths (OPLs) in the prefrontal cortex (PFC) at rest, using TRS. Methods: Employing TRS, we measured Hb concentrations and OPLs at rest in the PFC, and evaluated the relationship between the TRS parameters and cognitive function assessed by Mini-Mental State Examination (MMSE). In addition, we evaluated the relationship between the TRS parameters and the brain atrophy assessed by MRI. Results: We found positive correlations between MMSE scores and oxygen saturation (SO₂), oxy-Hb in the PFC, suggesting that the greater the degree of PFC activity, the higher the cognitive function. In addition, we found the negative correlation between the subject's age and SO₂ and oxy-Hb in the PFC, suggesting that the older the subject, the lower the PFC activity at rest. Moreover, the OPLs in the right PFC negatively correlated with degree of brain atrophy evaluated by MRI, indicating that the shorter the OPL, greater degree of brain atrophy. Conclusions: TRS allowed us to evaluate the relation between the cerebral blood oxygenation (CBO) in the PFC at rest and cognitive function.

Keywords: near infrared spectroscopy; aging; prefrontal cortex; TRS; magnetic resonance imaging; brain atrophy; VSRAD; optical pathlength; hemoglobin; cognitive function

1. Background

As the world's population is rapidly aging, dementia becomes a major global health problem. Currently, it is difficult to cure patients with progressive dementia, so emphasis is placed on early diagnosis and early intervention to prevent the onset of dementia [1]. The screening test of cognitive dysfunction, therefore, is important for early diagnosis of dementia. Currently, the Mini Mental State Examination (MMSE) is the most commonly used scale in cognitive function evaluation [2,3].

The MMSE is sensitive and cost-effective screening test; however, it is a subjective examination. Positron emission tomography (PET) and functional magnetic resonance imaging (fMRI) have been used for the diagnosis of dementia [4]; however, these techniques require large facilities and have high costs for examination and maintenance. A simple and less costly method to assess cognitive functions is still required for an objective screening test of dementia.

Near-infrared spectroscopy (NIRS), a non-invasive optical technique, appears to be an attractive alternative method since NIRS is compact and less expensive than fMRI or PET. NIRS evaluates cognitive functions by measuring evoked cerebral blood oxygenation (CBO) changes during cognitive tasks; NIRS provides concentration changes of oxyhemoglobin (oxy-Hb) and deoxyhemoglobin (deoxy-Hb) in cerebral vessels based on measurements of the absorption spectra of hemoglobin in the near-infrared wavelength range [5]. However, it should be noted that, in general, commercially available (conventional) NIRS systems employ continuous wave (CW) light allowing only qualitative measurements of relative changes in hemoglobin (Hb) concentrations during tasks [6]. Therefore, it is difficult to apply conventional CW-NIRS systems to evaluation of cognitive functions of aged people, particularly who cannot perform cognitive tasks due to dementia.

In contrast, time-resolved near infrared spectroscopy (TRS), which employs light sources of laser diodes emitting picosecond light pulses and a time-resolved detector with a picosecond time-resolution, can provide quantitative measurements of Hb concentrations as well as relevant optical parameters such as the absorption coefficient (μ_a), reduced scattering coefficient (μ_s') and optical pathlength (OPL) in the tissues interrogated by the light pulses [7,8]. μ_a and μ_s' are the optical properties averaged over the interrogated tissues and change mainly with the change in the HB concentration associated with the brain activation. OPL is the mean total optical pathlength of the light pulses travelling from the source to detector positions on the head surface, and it will change mainly with the change in the thicknesses of the various layers in the head tissues such as the scalp, cerebrospinal fluid (CSF), gray matter and white matter layers. One measurement procedure of TRS ends within a few minutes, and portable TRS systems cost much less than fMRI or PET. Because a TRS system used in this study is at an initial stage with an assumption of an optically homogeneous medium for multi-layered tissues of the human head, it can provide less spatial information than fMRI. Although the performance of the TRS system used in this study is limited, the measured HB concentrations and relevant optical parameters are very valuable for objective evaluation of dementia. Actually, TRS can measure hemodynamic conditions at rest due to its capability of acquiring baseline Hb concentrations quantitatively, and measurements at rest help evaluate the absolute changes in CBO from the rest to task states. By employing TRS in a previous study, we measured not only the Hb concentrations but also the OPLs in various regions of the brain of healthy adults [9]. In addition, for patients with subarachnoid hemorrhage (SAH), we measured baseline Hb concentrations at rest using TRS for detection of cerebral ischemia induced by vasospasms [10].

In the present study, by employing TRS, we focused on measuring the Hb concentrations and OPLs at rest in the prefrontal cortex (PFC) of patients under rehabilitation and investigated the relationship between the TRS parameters and cognitive functions assessed by the MMSE. In addition, we investigated the relationship between the TRS parameters and the brain atrophy assessed by MRI.

2. Methods

2.1. Subjects

We studied 202 subjects (87 males, 115 females; age 73.4 ± 13.0 years (mean \pm SD) who admitted to Southern Touhoku Kasuga Rehabilitation Hospital (Sukagawa city, Japan) for rehabilitation; 68.8% of the subjects suffered from cerebrovascular diseases including 79 cases of cerebral infarction, 41 cases of cerebral haemorrhage, 21 cases of subarachnoid haemorrhage. In addition, 94.6% of the subjects suffered from at least one life-style diseases. Tables 1 and 2 show the clinical profiles of patients and age distribution, respectively.

The subjects provided written informed consents as required by the Human Subjects Committee of the Rehabilitation Hospital. When the subject had a difficulty to understand the informed consent due to cognitive dysfunction, their family provided it.

Table 1. Clinical profiles of patients.

	Lifestyle-Related Diseases												Total
	HT	DM	HL	HT DM	HT HL	HT G	HL G	HT HL DM	HT HL DM G	HT DM G	HT HL G	none	
CH	18	1	0	6	6	0	0	6	1	0	0	3	41
SAH	9	0	4	1	3	0	0	3	0	0	0	1	21
CI	16	3	6	12	10	2	2	14	1	1	5	7	79
HI	2	0	0	0	0	0	0	0	0	0	0	1	3
BF	16	1	0	4	4	0	0	2	0	0	0	12	39
others	8	0	0	4	0	0	0	1	0	1	1	4	19
Total	69	5	10	27	23	2	2	26	2	2	6	28	202

HT = Hypertension, DM = Diabetes Mellitus, HL = Hyperlipidemia, G = Gout CH = Cerebral hemorrhage, SAH = Subarachnoid hemorrhage, CI = Cerebral infarction, HI = Head injury, BF = Born fracture.

Table 2. Distribution of patient’s age.

Age	Male	Female	Total
≤50	11	4	15
51–60	15	8	23
61–70	20	14	34
71–80	19	38	57
≥80	22	51	73
total	87	115	202

2.2. TRS Measurement

We tried to measure Hb concentrations at rest in the bilateral PFC with a two-channel TRS system (TRS-20, Hamamatsu Photonics K.K., Hamamatsu, Japan). Details of this system have been described [11]. Briefly, it consists of three pulsed laser diodes with different wavelengths (761 nm, 791 nm, and 836 nm) having a pulse duration of 100 ps at a repetition frequency of 5 MHz, a photomultiplier tube (PMT; H6279-MOD, Hamamatsu Photonics K.K., Japan), and a circuit for time-resolved measurement based on the time-correlated single photon counting technique.

Two optical probes having a pair of source and detector optical fibers each of the two-channel TRS system were attached onto the forehead with a bilateral symmetry using a flexible fixation pad, so that the midpoints between the source and detector positions were 30 mm above the centers of the upper edges of the bilateral orbital sockets. The distance between the source and detector of each probe was set at 40 mm. These positionings of the midpoints are similar to those of the midpoints between electrode positions Fp1/F3 (left) and Fp2/F4 (right) of the international electroencephalographic 10–20 system. MRI images confirmed that the optical probes were located over the dorsolateral and frontopolar areas of the PFC. Based on a simulation study of photon migration in the adult head [12], we believe that the TRS measurements in this study provided the CBO changes in the surface region of the PFC under the two midpoints between the source and detector positions.

The TRS system acquired time-resolved reflectances using the two probes. From the acquired time-resolved reflectances, various parameters were obtained assuming that the interrogated forehead tissue was an optically homogeneous semi-infinite medium with the absorption and reduced scattering coefficients of $\mu_a(\lambda)$ and $\mu_s'(\lambda)$ for the wavelength of λ , respectively. The time-resolved reflectance

derived from the analytical solution of the photon diffusion equation for a homogeneous semi-infinite medium is given by Equation (1) under the zero-boundary condition [8],

$$R(t, \rho; \lambda) = \frac{z_0}{(4\pi Dc)^{3/2} t^{5/2}} \exp[-\mu_a(\lambda)ct] \exp\left(-\frac{\rho^2 + z_0^2}{4Dct}\right), \quad (1)$$

where $R(t, \rho; \lambda)$ is the time-resolved reflectance at time of t with the distance between the source and detector positions of ρ ($= 40$ mm) for the wavelength of λ , c is the speed of light in the tissue, D is the diffusion coefficient given as $1/[3\mu_s'(\lambda)]$, and $z_0 = 1/\mu_s'(\lambda)$. Here the wavelength dependences of D and z_0 are omitted for simplicity. Equation (1), convoluted by the instrumental response function of TRS-20, was fitted to the measured time-resolved reflectance to estimate $\mu_a(\lambda)$ and $\mu_s'(\lambda)$ of the medium using a non-linear least-squared technique. The absorption coefficient of tissue was assumed to be the sum of the absorption coefficients of oxy-Hb, deoxy-Hb and background tissue as Equation (2),

$$\mu_a(\lambda) = \varepsilon_{oxy-Hb}(\lambda)C_{oxy-Hb} + \varepsilon_{deoxy-Hb}(\lambda)C_{deoxy-Hb} + \mu_{a,BG}(\lambda) \quad (2)$$

where $\varepsilon(\lambda)$ and C are the extinction (or molar absorption) coefficient and the molar concentration, respectively, with the subscript indicating oxy-Hb, deoxy-Hb or background tissue. Solving the simultaneous equations of Equation (2) for the three wavelengths (761 nm, 791 nm, and 836 nm) gave the concentrations of oxy-Hb (C_{oxy-Hb}), deoxy-Hb ($C_{deoxy-Hb}$) and total-Hb ($C_{t-Hb} = C_{oxy-Hb} + C_{deoxy-Hb}$). Then the oxygen saturation, $SO_2 = C_{oxy-Hb}/C_{t-Hb}$, was calculated. The unit of the concentrations of oxy-Hb and deoxy-Hb are μM . The mean total optical pathlength of the detected light for the wavelength of λ , $OPL(\lambda)$, was calculated by Equation (3),

$$OPL(\lambda) = \frac{c \int_0^{\infty} tR(t, \rho; \lambda)dt}{\int_0^{\infty} R(t, \rho; \lambda)dt} \quad (3)$$

It should be noted that the Hb concentrations and SO_2 obtained by Equations (2) and (3) are the averages over the whole regions interrogated by the light pulses, and for separating those of the individual layers, i.e., the scalp, CSF, gray and white matter layers, it is necessary to know the partial optical pathlengths of the individual layers. Although it is very difficult to know the partial optical pathlengths of the individual layers, from the reference [12] the partial optical pathlength of the cortex, mainly the gray matter, is estimated to be about 5 to 10 % of the OPL. Therefore, the Hb concentrations and SO_2 of the cortex occupy only 5 to 10% of those obtained by this study using Equations (2) and (3).

2.3. Assessment of Cognitive Function

We evaluated cognitive functions of the subjects using the MMSE, which is effective as a screening tool that can be used to systematically assess mental status [2]. It was reported that sociocultural variables, ages and education could affect individual MMSE scores [13,14]; however, traditionally, a 23/24 cut off has been used to select patients with suspected cognitive impairment or dementia [15]. In the present study, the mean MMSE scores of all subjects were 24.8 ± 4.6 ; 108 cases for suspected normal (MMSE ≥ 24), 94 cases for suspected cognitive impairment or dementia (MMSE ≤ 23).

2.4. MRI

55 subjects underwent an MRI study on a 1.5T Vision Plus imager (Siemens, Erlangen, Germany). One hundred forty 3D sections of a T1-weighted magnetization-prepared rapid acquisition of gradient echo sequence were obtained in a sagittal orientation as 1.2-mm thick sections (FOV $_ 23$, TR $_ 9.7$ ms, TE $_ 4$ ms, flip angle $_ 12^\circ$, and TI $_ 300$ ms, with no intersection gaps).

We analyzed the morphological changes of the brain using the voxel-based specific regional analysis system for Alzheimer’s disease (VSRAD), a diagnosis-aiding program, which runs on Windows, for voxel-based morphometry based on statistical parametric mapping (SPM8) and diffeomorphic anatomical registration using the exponentiated lie (DARTEL) [16]. VSRAD is widely used in current clinical practice in the treatment of AD [17].

VSRAD generates the following scores [16]: (1) Severity; the severity of atrophy obtained from the averaged positive z score in the target volume of interest (VOI) (i.e., hippocampus and its surroundings); (2) Extent of VOI atrophy (%); the extent of a region showing significant atrophy in the target VOI—that is, the percentage rate of the coordinates with a z value exceeding the threshold value of 2 in the target VOI; (3) Ratio; the extent of a region showing significant atrophy in the whole brain—that is, the percentage rate of the coordinates with a z value exceeding the threshold value of 2 in the whole brain; (4) Whole Brain Extent (%); the ratio of the extent of a region showing significant atrophy in the target VOI to the extent of a region showing significant atrophy in the whole brain.

2.5. Data Analysis

We evaluated correlations between ages, the MMSE scores, VSRAD scores, Hb concentrations and OPLs measured by TRS, employing Pearson’s correlation analysis.

3. Results

3.1. Correlations between MMSE Scores and Subject’s Age

The patients exhibited a variety of cognitive functions between normal and dementia; the mean MMSE scores were 25.3 ± 4.0 . There was a significant negative correlation between the MMSE score and patient’s age ($r = -0.48$, $p < 0.01$), indicating that the MMSE score decreases with age.

3.2. Correlations Between TRS Parameters and MMSE Scores, Subject’s Age

TRS measurements revealed significant positive correlations between the MMSE score and SO_2 in the bilateral PFC ($r = 0.40$, $p < 0.01$). In addition, C_{oxy-Hb} ($r = 0.23$, $p < 0.01$) and C_{t-Hb} ($r = 0.14$, $p < 0.05$) in the right PFC exhibited significant positive correlations with the MMSE scores. In contrast, $C_{deoxy-Hb}$ in the left PFC exhibited a significant negative correlation with the MMSE score ($r = -0.19$, $p < 0.01$). Moreover, SO_2 and C_{oxy-Hb} in the bilateral PFC exhibited negative correlations with age.

However, OPL in the PFC did not exhibit significant correlations with the MMSE score and patient’s age ($p > 0.05$). Table 3 summarizes the correlations between the MMSE scores, subject’s ages, Hb concentrations and SO_2 at rest in the PFC.

Table 3. Correlations between the MMSE score, subject’s ages, Hb concentrations and SO_2 at rest in the right and left PFC ($n = 202$).

		Age	MMSE
Right PFC	C_{oxy-Hb} [μ M]	−0.196 **	0.230 **
	$C_{deoxy-Hb}$ [μ M]	0.029	−0.047
	C_{t-Hb} [μ M]	−0.127	0.142 *
	SO_2 [%]	−0.270 **	0.396 **
Left PFC	C_{oxy-Hb} [μ M]	−0.189 **	0.135
	$C_{deoxy-Hb}$ [μ M]	0.084	−0.191 **
	C_{t-Hb} [μ M]	−0.107	0.022
	SO_2 [%]	−0.302 **	0.398 **

* indicates $p < 0.05$. ** indicates $p < 0.01$.

3.3. Correlations between VSRAD Parameters and MMSE Scores, Subject's Age

There were negative correlations between the MMSE scores and the VSRAD scores including Severity ($r = -0.453, p < 0.01$), Extent ($r = -0.484, p < 0.01$), Ratio ($r = -0.402, p < 0.01$), and Whole Brain Extent ($r = -0.409, p < 0.01$). In contrast, the subject's age positively correlated with the VSRAD scores including Severity ($r = 0.406, p < 0.01$), Extent ($r = 0.476, p < 0.01$), Ratio ($r = 0.400, p < 0.01$), and Whole Brain Extent ($r = 0.404, p < 0.01$) (Table 4).

Table 4. Correlations between VSRAD parameters and MMSE scores, subject's age.

	VSRAD			
	Severity	Brain Extent (%)	Extent (%)	Ratio
Age	0.406 **	0.404 **	0.476 **	0.400 **
MMSE	-0.453 **	-0.409 **	-0.484 **	-0.402 **

* indicates $p < 0.05$. ** indicates $p < 0.01$.

3.4. Correlations between OPL and VSRAD Parameters

The degree of brain atrophy affected the OPLs. Figure 1 compares MRI images (fluid attenuated IR) of subjects with no brain atrophy (A) and severe brain atrophy (B). Table 5A compares the MMSE scores and VRSAD scores between no brain atrophy (Case A) and severe brain atrophy (Case B). The subarachnoid space in case B is larger than that in case A due to brain atrophy. Interestingly, the OPLs in case B were shorter than those in case A (Table 5B).

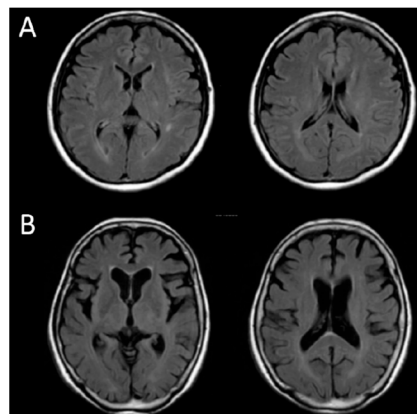


Figure 1. MRI images (fluid attenuated IR) of subjects with (A) no brain atrophy and (B) severe brain atrophy.

Table 5A. Comparison of VRSAD scores between no brain atrophy (Case A) and severe brain atrophy (Case B).

Case	Age/sex	MMSE	Severity	Whole Brain Extent (%)	Extent of VOI atrophy (%)	Ratio
A	50/F	30	0.27	1.40	0.00	0.00
B	77/F	9	3.48	6.48	86.17	13.29

VOI indicates Volume of interest.

Table 5B. Comparison of OPLs (in mm) between no brain atrophy (Case A) and severe brain atrophy (Case B).

Case	Right			Left			Average
	OPL1 (761 nm)	OPL2 (791 nm)	OPL3 (836 nm)	OPL1 (761 nm)	OPL2 (791 nm)	OPL3 (836 nm)	
A	217.9	220.8	208.4	226.2	227.2	211.4	218.7 (1.00)
B	177.1	179.0	169.6	171.8	174.0	162.9	172.4 (0.79)

On average, the OPLs (761 nm, 791 nm, and 836 nm) in the right PFC negatively correlated with VSRAD scores including Severity, Extent, and Ratio, but not Whole Brain Extent. In contrast, the correlations between the OPLs in the left PFC and VSRAD scores were limited. Table 6 summarizes the correlations between the OPLs and VSRAD scores.

Table 6. Correlations between OPLs and VSRAD parameters.

		VSRAD			
		Severity	Whole Brain Extent (%)	Extent of VOI Atrophy (%)	Ratio
Right PFC	OPL1	−0.305 *	0.073	−0.312 *	−0.396 **
	OPL2	−0.284 *	0.095	−0.292 *	−0.386 **
	OPL3	−0.306 *	0.052	−0.312 *	−0.395 **
Left PFC	OPL1	−0.211	−0.038	−0.242	−0.248
	OPL2	−0.228	−0.023	−0.262	−0.283 *
	OPL3	−0.240	−0.038	−0.276 *	−0.294 *

* indicates $p < 0.05$. ** indicates $p < 0.01$.

4. Discussion

In the present study using TRS, we evaluated the relationship between the cognitive functions (i.e., the MMSE scores) and optical parameters of the head regions including the PFC in elderly subjects with systemic disorders. It is difficult to measure Hb concentrations in the cortex selectively by TRS; however, the following findings suggest that the Hb concentrations measured by TRS reflected CBO in the PFC. First, simultaneous measurements of TRS and PET demonstrated that C_{t-Hb} and SO_2 measured by TRS correlated with an increase of regional cerebral blood flow and volume induced by acetazolamide [18]. Second, the result of TRS functional study was consistent with the result obtained by fMRI; TRS demonstrated an increase in $C_{deoxy-Hb}$ in the PFC during driving simulation while fMRI demonstrated a decrease in the Blood oxygenation level dependent (BOLD) signal (i.e., deactivation) in the PFC [19]. Third, TRS could detect cerebral ischemia caused by vasospasms after SAH by demonstrating a decrease in C_{oxy-Hb} and SO_2 [10]. These findings suggest that C_{oxy-Hb} and SO_2 measured by TRS at rest reflected the PFC activity at rest.

The present study revealed positive correlations between the MMSE score and SO_2 , C_{oxy-Hb} in the PFC, suggesting that the greater the degree of PFC activity at rest, the higher the cognitive function. These observations are consistent with our recent TRS study on elderly women, which demonstrated that mild cognitive impairment exhibited higher baseline C_{oxy-Hb} in the PFC than those in severe cognitive impairment [20]. Moreover, the negative correlation between the subject’s age and SO_2 and C_{oxy-Hb} in the PFC suggest that the older the subject, the lower the PFC activity at rest, which is consistent with the studies on the effect of aging on regional cerebral blood flow in the PFC [21].

The close correlations between the MMSE score and the TRS parameters suggest that machine learning may allow prediction of cognitive function based on the TRS parameters. For the prediction, deep learning, a subset of machine learning, may be useful since it allows analyzing regularity and relevance from a large amount of data, make judgments and predictions [22]. Indeed, the deep learning has been applied to imaging diagnosis [23], including computer- aided-diagnosis of Alzheimer’s Disease (AD) based on MRI images [24]. In our preliminary study, we evaluated the variable importance for the prediction, and found that the subject’s age showed the highest rank (1.0) while the right and left SO2 showed the second (0.77) and third (0.73) highest rank, respectively [25]. It should be noted that these parameters with high variable importance showed high correlation coefficients. Combination of MRI image and TRS measurement may be useful to predict cognitive dysfunction. In order to develop a deep learning based-diagnostic method of cognitive dysfunction, further study is necessary based on the present study.

The OPLs in the right PFC negatively correlated with VSRAD scores (Severity, Extent, and Ratio), indicating that the shorter the OPL, the greater the VSRAD scores which means greater degree of brain atrophy [16,17]. This might be caused by an increase of subarachnoid space due to brain atrophy; an increase of cerebrospinal fluid (CSF) layer in subarachnoid space caused a shortening of OPL since light scattering of CSF is much less than that of brain tissue. However, these findings are inconsistent with our previous TRS study on chronic stroke patients; we observed that the OPLs on the affected side, where subarachnoid space increased due to cortical atrophy in chronic stroke, was longer than that on the normal side [26]. It should be noted, however, that VSRAD scores does not indicate the degree of the PFC atrophy selectively. Therefore, further study, such as selective measurements of the degree of atrophy of the PFC, is necessary to clarify the relation between OPLs and brain atrophy.

Interestingly, there was a difference in correlation of OPLs and VSRAD between left and right PFC. Some evidence suggests that neurodegeneration related to aging and disease may preferentially affect the left-usually language- and motor-dominant-hemisphere; however, a recent meta-analysis provided no evidence for increased left-hemisphere vulnerability [27]. Further work is needed to provide a better understanding of the role of gray matter asymmetries.

We discuss the relation between the brain atrophy and the OPL from the view point of light propagation in the head. According to the numerical study of light propagation inside a human head model by Koyama et al. [28], the OPL between the source and detector depends on the reduced scattering coefficient of the CSF layer (μ'_{s-CSF}), which corresponds to the subarachnoid space. The head model consists of four layers, i.e., the superficial layer including the scalp and skull (thickness of 10 mm), the CSF layer (2 mm), the gray matter (4 mm) and the white matter (6 mm). Light injected from the source propagates through the four layers to reach the detector with the partial optical pathlengths of l_{sup} , l_{CSF} , l_{gray} and l_{white} in the four layers, respectively, and the OPL is the sum of all the partial optical pathlengths, $OPL = l_{sup} + l_{CSF} + l_{gray} + l_{white}$. As the results of their numerical calculation, for the case of the source-detector distance of $\rho = 40$ mm, the OPL decreases with the decrease in μ'_{s-CSF} as shown in Table 7.

Table 7. Changes in the total and partial optical pathlengths with the change in μ'_{s-CSF} of the CSF layer for the case of the source-detector distance of $\rho = 40$ mm. Data from [28].

μ'_{s-CSF} (mm ⁻¹)	OPL (mm)	l_{sup} (mm)	l_{CSF} (mm)	l_{gray} (mm)	l_{white} (mm)
1.0 (soft tissue)	320	268	35	16	0.5
0.3 (weak scat.)	298	224	51	22	0.6
0.01 (very weak scat.)	239	170	53	16	0.4

While the OPL and l_{sup} decrease with the decrease in μ'_{s-CSF} , l_{CSF} and l_{gray} increase with the decrease in μ'_{s-CSF} . The results can be understood phenomenologically as the following. When $\mu'_{s-CSF} = 1.0$ mm⁻¹, the CSF layer exhibits strong scattering similarly to that of soft tissue, and the light

propagation pattern inside the head model can be schematically described as in Figure 2a where the thickness of the CSF layer is exaggerated to see its effect on light propagation. The propagation path from the source, S, to the detector, D, depicts a so-called banana shape as a semitransparent yellow region. In this case, the typical propagation path expressed by the red zig-zag lines crosses the interface between the superficial and CSF layers at positions “a” and “d” with a relatively short distance between them.

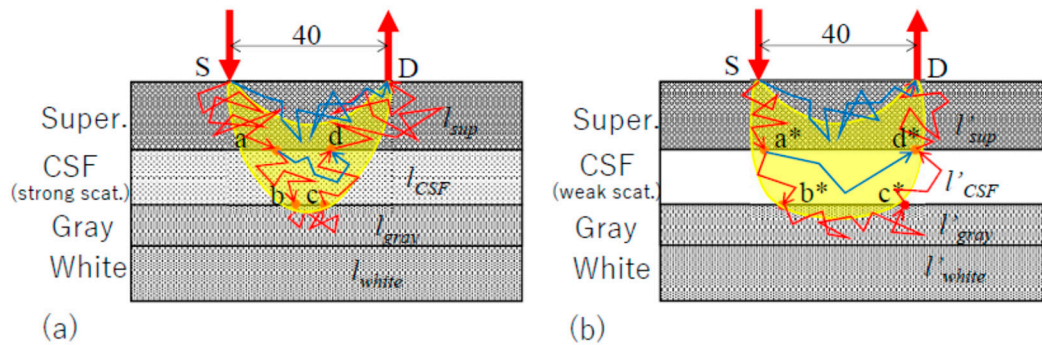


Figure 2. Patterns of light propagation in the head model with (a) $\mu'_{s\text{-CSF}} = 1.0 \text{ mm}^{-1}$ (strong scattering as soft tissue) and (b) $\mu'_{s\text{-CSF}} = 0.01 \text{ mm}^{-1}$ (very weak scattering).

When $\mu'_{s\text{-CSF}} = 0.01 \text{ mm}^{-1}$, the CSF layer exhibits very weak (or almost no) scattering, and the light propagation pattern can be described as in Figure 2b. The propagation pattern in Figure 2b is widened from the banana shape in Figure 2a due to the presence of the almost non-scattering CSF layer, and the typical propagation path crosses the interface between the superficial and CSF layers at positions “a*” and “d*” with a longer distance between them than the distance between “a” and “d”. Because light in the CSF layer propagates a long distance without being scattered, a part of light propagating in the superficial layer can circumvent the strong scattering superficial layer by going through the CSF layer to reach the detector, D. Resultantly, l_{sup} decreases while l_{CSF} increases although the decrease in l_{sup} is much larger than the increase in l_{CSF} . This is the reason why the OPL decreases with the decrease in $\mu'_{s\text{-CSF}}$ in Table 6.

The results of Table 6 do not describe the relationship between the OPL and $\mu'_{s\text{-CSF}}$ but that between the OPL and the extent of VOI atrophy. However, the decrease in the $\mu'_{s\text{-CSF}}$ can be understood to be equivalent to the increase in the extent of Volume of interest (VOI) atrophy. Nevertheless, there is still a possibility that more precise simulation of light propagation in the human head with increasing or decreasing thickness of the CSF layer may provide the opposite results to those described above, i.e., the OPL increases with the increase in the thickness of the CSF layer. Further investigation about the relation between the OPL and the thickness of the CSF layer is necessary.

5. Conclusions

The present study demonstrated that TRS may be applicable to assessment of cognitive dysfunction, since Hb concentrations measured by TRS at rest in the PFC correlated with cognitive functions evaluated by the MMSE. It should be emphasized that TRS measurements at resting condition may be useful in aged people, particularly subjects with cognitive dysfunction who cannot perform cognitive tasks. In contrast to activation methods, the present method does not allow us to investigate the type of cognitive function being impaired by changing the type of task. However, TRS may be applicable to screening test of cognitive impairment; our preliminary study demonstrated that deep learning allows to predict the MMSE scores based on the TRS parameters [25,29].

Author Contributions: K.S. designed the study, and wrote the initial draft of the manuscript. L.H. and N.O. contributed to analysis and interpretation of data, assisted in the preparation of the manuscript. Y.Y. contributed to interpretation of TRS data, and critically reviewed the manuscript. All authors approved the final version of the manuscript, and agree to be accountable for all aspects of the work in insuring that questions related to the accuracy of integrity of any part of the work are appropriately investigated and resolved.

Funding: This work was supported in part by a Grant-in-Aid from the Ministry of Education, Culture, Sports, Sciences and Technology of Japan (Strategic Research Foundation Grant-aided Project for Private Universities S1411017), JSPS Grant-in-Aid for Young Scientists (B, 16K16077), from MEXT of Japan, and Ministry of Economy, Trade and Industry (Groundwork Project for Creating Industrial Models Using IoT)

Conflicts of Interest: The authors declare no conflict of interest.

References

- Livingston, G.; Sommerlad, A.; Orgeta, V.; Costafreda, S.G.; Huntley, J.; Ames, D.; Ballard, C.; Banerjee, S.; Burns, A.; Cohen-Mansfield, J.; et al. Dementia prevention, intervention, and care. *Lancet* **2017**, *390*, 2673–2734. [[CrossRef](#)]
- Folstein, M.F.; Folstein, S.E.; McHugh, P.R. “Mini-mental state”. A practical method for grading the cognitive state of patients for the clinician. *J. Psychiatr. Res.* **1975**, *12*, 189–198. [[CrossRef](#)]
- Arevalo-Rodriguez, I.; Smailagic, N.; Roqué, I.; Figuls, M.; Ciapponi, A.; Sanchez-Perez, E.; Giannakou, A.; Pedraza, O.L.; Bonfill Cosp, X.; Cullum, S. Mini-Mental State Examination (MMSE) for the detection of Alzheimer’s disease and other dementias in people with mild cognitive impairment (MCI). *Cochrane Database Syst. Rev.* **2015**, *3*, CD010783.
- Scheltens, P.; Blennow, K.; Breteler, M.M.; de Strooper, B.; Frisoni, G.B.; Salloway, S.; Van der Flier, W.M. Alzheimer’s disease. *Lancet* **2016**, *388*, 505–517. [[CrossRef](#)]
- Jöbsis, F.F. Noninvasive, infrared monitoring of cerebral and myocardial oxygen sufficiency and circulatory parameters. *Science* **1977**, *198*, 1264–1267. [[CrossRef](#)]
- Reynolds, E.O.; Wyatt, J.S.; Azzopardi, D.; Delpy, D.T.; Cady, E.B.; Cope, M.; Wray, S. New non-invasive methods for assessing brain oxygenation and hemodynamics. *Br. Med. Bull.* **1988**, *44*, 1052–1075. [[CrossRef](#)]
- Chance, B.; Leigh, J.S.; Miyake, H.; Smith, D.S.; Nioka, S.; Greenfeld, R.; Finander, M.; Kaufmann, K.; Levy, W.; Young, M. Comparison of time-resolved and -unresolved measurements of deoxyhemoglobin in brain. *Proc. Natl. Acad. Sci. USA* **1988**, *85*, 4971–4975. [[CrossRef](#)] [[PubMed](#)]
- Patterson, M.S.; Chance, B.; Wilson, C. Time resolved reflectance and transmittance for the non-invasive measurement of tissue optical properties. *Appl. Opt.* **1989**, *28*, 2331–2336. [[CrossRef](#)] [[PubMed](#)]
- Katagiri, A.; Dan, I.; Tuzuki, D.; Okamoto, M.; Yokose, N.; Igarashi, K.; Hoshino, T.; Fujiwara, T.; Katayama, Y.; Yamaguchi, Y.; et al. Mapping of optical pathlength of human adult head at multi-wavelengths in near infrared spectroscopy. *Adv. Exp. Med. Biol.* **2010**, *662*, 205–212.
- Yokose, N.; Sakatani, K.; Murata, Y.; Awano, T.; Igarashi, T.; Nakamura, S.; Hoshino, T.; Katayama, Y. Bedside monitoring of cerebral blood oxygenation and hemodynamics after aneurysmal subarachnoid hemorrhage by quantitative time-resolved near-infrared spectroscopy. *World Neurosurg.* **2010**, *73*, 508–513. [[CrossRef](#)]
- Oda, M.; Nakano, T.; Suzuki, A.; Shimomura, F.; Suzuki, T. Near infrared time-resolved spectroscopy system for tissue oxygenation monitor. *SPIE* **2000**, *4160*, 204–210.
- Okada, E.; Delpy, D.T. Near-infrared light propagation in an adult head model. I. Modeling of low-level scattering in the cerebrospinal fluid layer. *Appl. Opt.* **2003**, *42*, 2906–2914. [[CrossRef](#)]
- Brayne, C.; Calloway, P. The association of education and socioeconomic status with the Mini Mental State Examination and the clinical diagnosis of dementia in elderly people. *Age Ageing* **1990**, *19*, 91–96. [[CrossRef](#)]
- Crum, R.M.; Anthony, J.C.; Bassett, S.S.; Folstein, M.F. Population-based norms for the Mini-Mental State Examination by age and educational level. *JAMA* **1993**, *269*, 2386–2391. [[CrossRef](#)] [[PubMed](#)]
- Tombaugh, T.N.; McIntyre, N.J. The mini-mental state examination: A comprehensive review. *J. Am. Geriatr. Soc.* **1992**, *40*, 922–935. [[CrossRef](#)] [[PubMed](#)]
- Matsuda, H.; Mizumura, S.; Nemoto, K.; Yamashita, F.; Imabayashi, E.; Sato, N. Automatic voxel-based morphometry of structural MRI by SPM8 plus diffeomorphic anatomic registration through exponentiated lie algebra improves the diagnosis of probable Alzheimer Disease. *Am. J. Neuroradiol.* **2012**, *33*, 1109–1114. [[CrossRef](#)]

17. Matsuda, H. Voxel-based Morphometry of Brain MRI in Normal Aging and Alzheimer's Disease. *Aging Dis.* **2013**, *4*, 29–37. [[PubMed](#)]
18. Ohmae, E.; Ouchi, Y.; Oda, M. Cerebral hemodynamics evaluation by near-infrared time-resolved spectroscopy: Correlation with simultaneous positron emission tomography measurements. *NeuroImage* **2006**, *29*, 697–705. [[CrossRef](#)]
19. Sakatani, K.; Yamashita, D.; Yamanaka, T. Changes of cerebral blood oxygenation and optical pathlength during activation and deactivation in the prefrontal cortex measured by time-resolved near infrared spectroscopy. *Life Sci.* **2006**, *78*, 2734–2741. [[CrossRef](#)]
20. Machida, A.; Shirato, M.; Tanida, M.; Kanemaru, C.; Nagai, S.; Sakatani, K. Effects of Cosmetic Therapy on Cognitive Function in Elderly Women Evaluated by Time-Resolved Spectroscopy Study. *Adv. Exp. Med. Biol.* **2016**, *876*, 289–295. [[PubMed](#)]
21. Martin, A.J.; Friston, K.J.; Colebatch, J.G.; Frackowiak, R.S. Decreases in regional cerebral blood flow with normal aging. *J. Cereb. Blood Flow Metab.* **1991**, *11*, 684–689. [[CrossRef](#)]
22. Sze, V.; Chen, Y.H.; Yang, T.J.; Joel, S. Efficient Processing of Deep Neural Networks: A tutorial and Survey. *Proc. IEEE* **2017**, *105*, 2295–2329. [[CrossRef](#)]
23. Hosny, A.; Parmar, C.; Quackenbush, J.; Schwartz, L.H.; Aerts, H.J.W.L. Artificial intelligence in radiology. *Nat. Rev. Cancer* **2018**, *18*, 500–510. [[CrossRef](#)]
24. Liu, S.; Liu, S.; Cai, W.; Pujol, S.; Kikinis, R.; Feng, D. Early diagnosis of Alzheimer's disease with deep learning. In Proceedings of the 2014 IEEE 11th International Symposium on Biomedical Imaging (ISBI), Beijing, China, 29 April–2 May 2014; pp. 1015–1018.
25. Oyama, K.; Hu, L.; Sakatani, K. Prediction of MMSE score using time-resolved near-infrared spectroscopy. In Proceedings of the 45th Annual Meeting of the International Society on Oxygen Transport to Tissue (ISOTT), Halle, Germany, 19–23 August 2017.
26. Sato, Y.; Komuro, Y.; Lin, L.; Tang, Z.; Hu, L.; Kadowaki, S.; Ugawa, Y.; Yamada, Y.; Sakatani, K. Differences in Tissue Oxygenation, Perfusion and Optical Properties in Brain Areas Affected by Stroke: A Time-Resolved NIRS Study. *Adv. Exp. Med. Biol.* **2018**, *1072*, 63–67.
27. Minkova, L.; Habich, A.; Peter, J.; Kaller, C.P.; Eickhoff, S.B.; Klöppel, S. Gray matter asymmetries in aging and neurodegeneration: A review and meta-analysis. *Hum. Brain Mapp.* **2017**, *38*, 5890–5904. [[CrossRef](#)]
28. Koyama, T.; Iwasaki, A.; Ogoshi, Y.; Okada, E. Practical and adequate approach to modeling light propagation in an adult head with low-scattering regions by use of diffusion theory. *Appl. Opt.* **2005**, *44*, 2094–2103. [[CrossRef](#)]
29. Oyama, K.; Hu, L.; Sakatani, K. Prediction of MMSE score using time-resolved near-infrared spectroscopy. *Adv. Exp. Med. Biol.* **2018**, *1072*, 145–150.



© 2019 by the authors. Licensee MDPI, Basel, Switzerland. This article is an open access article distributed under the terms and conditions of the Creative Commons Attribution (CC BY) license (<http://creativecommons.org/licenses/by/4.0/>).